Glacial isostatic adjustment in Fennoscandia with a three-dimensional viscosity structure as an inverse problem

Georg Kaufmann [a,*], Patrick Wu [b]

[a] *Institut für Geophysik, Universität Göttingen, Herzberger Landstr. 180, 37075 Göttingen, Germany*
[b] *Department of Geology and Geophysics, University of Calgary, Calgary, AB, Canada T2N 1N4*

Abstract

Glacial isostatic adjustment data are commonly used to invert for the radial viscosity structure of the mantle. However, the effects of lateral variations in mantle viscosity in such inversions are not yet accounted for. Here we analysed synthetic sea-level data for the Fennoscandian region, which are derived from a three-dimensional (3D) earth model with realistic lateral and vertical viscosity variations deduced from seismological and geological information. The inversion of the 3D synthetic data for a best-fitting 1D viscosity profile reveals that (i) lateral lithospheric thickness variations can be detected with 1D model predictions, if the data are grouped into regional subsets, (ii) combined lateral variations in lithospheric thickness and asthenospheric viscosity are not properly resolved with 1D model predictions, and (iii) the spatial and temporal distribution of observational data strongly affects the resulting 1D viscosity profile. © 2002 Elsevier Science B.V. All rights reserved.

1. Introduction

The glacial isostatic adjustment of the Earth as a result of mass redistributions during the ice-age cycles is successfully modelled within the framework of global glacial isostatic adjustment theory [1–4]. However, while the complex three-dimensional (3D) variation of the combined ice and water load is fully taken into account [5–7], the properties of the Earth's crust and mantle are assumed to vary in the radial direction only. This latter assumption, which simplifies the modelling procedure significantly, ignores the complex 3D structure of the Earth's interior as seen by seismic tomographical imaging [8–10].

Several studies have been carried out in the past to infer the effects of lateral variations in mantle properties on observations related to the glacial isostatic adjustment process. While most of these studies, based on simple axisymmetrical ice load histories, were intended to assess the effects of some 3D variations in the Earth's mantle in general [11–17] studies on more realistic, fully 3D ice and earth models are rare [18–21].

Our own results from solving the forward problem of glacial isostatic adjustment on a 3D earth

* Corresponding author.
Tel.: +49-551-397462; Fax: +49-551-397459.
E-mail address: gkaufman@uni-geophys.gwdg.de (G. Kaufmann).

[13,15,18,20] suggest that lateral variations in lithospheric thickness alone result in modelling differences for relative sea-levels (RSLs) around $\Delta RSL \sim 10$ m, when compared to radially symmetric earth model predictions. We have derived a least-squares (χ^2) misfit between model predictions and observational data, and the reduction in χ^2-misfit for RSL data is good ($\chi^2 < 1$). The best model found reflects the *average* lithospheric thickness, and lateral lithospheric variation *can* be detected with 1D models.

When both lateral variations in lithospheric thickness and asthenospheric viscosity are taken into account, modelling differences for RSLs are around $\Delta RSL \sim 20$ m in the peripheral areas and $\Delta RSL \sim 100$ m in the central areas. However, the reduction in χ^2-misfit is less good ($\chi^2 \simeq 2$), and the best-fitting 1D model results in *wrong* lithospheric thickness and asthenospheric viscosity values. Hence, the correct asthenospheric viscosity variation cannot be detected with 1D models.

In [17], a 2D earth model with a thick continental root underneath a parabolic ice sheet of the size of the Fennoscandian Ice Sheet and a thinner lithosphere outside the glaciated area with an underlying low-viscosity asthenosphere has been used to generate synthetic sea-level data. The authors then inverted the synthetic data for the best-fitting 1D viscosity profile, but the low-viscosity asthenosphere was not recovered with the best 1D viscosity models.

In this paper, we extend our previous results by following a different approach: as in [17], we formulate the inverse problem by calculating synthetic sea-level data from a 3D earth model for Fennoscandia, whose vertical and lateral viscosity distribution is derived from seismological and geological information. We then analyse the response of 1D earth models based on vertical viscosity variations only by comparing the 1D response to the 3D synthetic data. We use realistic RSL data from the Fennoscandian region, with their irregular distribution of sea-level sites, sampling times, and observational uncertainties, and replace the observed sea-level data by our synthetic 3D earth model predictions. This approach enables us to study the limiting resolution of a real data set on the inverse inferences of the 1D

mantle viscosity profiles. The advantage of this approach is to gain valuable insight into uncertainties in modelling, if the 3D nature of the earth is neglected. We also investigate the effect of spatial and temporal distribution of observational data on the resulting viscosity structure.

2. Models

2.1. Earth models

A layered, isotropic, compressible, Maxwell-viscoelastic half-space with a constant gravitational attraction of $g = 9.81$ m s^{-2} is used to model the glacially induced perturbations of the solid Earth in the Fennoscandian region. As shown earlier [22,23], the flat-earth approximation is adequate to describe the glacial isostatic adjustment for an ice model of the size of the former Late Pleistocene ice cover over Fennoscandia. We solve the Boussinesq problem for a layered, viscoelastic half-space using the commercial finite-element package Abaqus, which has been modified to include pre-stress advection in order to allow the deformed free surface to return to its initial equilibrium via viscous flow [24,25]. Thus, the equation that describes the conservation of momentum is given by:

$$\nabla \cdot \sigma - \rho g \nabla w = 0 \qquad (1)$$

where σ is the incremental stress tensor, ρ the density, g the gravitational acceleration, and w is the vertical displacement. The first term in Eq. 1, the divergence of stress, describes the surface force deforming the Earth. The second term arises because the undisturbed Earth is assumed to be in hydrostatic equilibrium, with the gravitational forces balanced by the hydrostatic pre-stress. This pre-stress is being advected along with the material when the body deforms either elastically or viscoelastically. Thus, the second term in Eq. 1 represents the gradient of the advected pre-stress, ρgw. The presence of this term is required in order to provide the buoyancy force that is needed to satisfy the boundary conditions in the fluid limit, and without this term, there would be no viscous
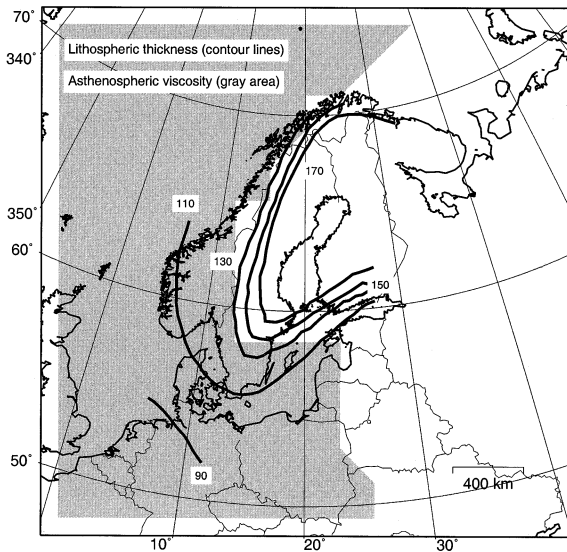
Fig. 1. Lateral variation underneath Fennoscandia in lithospheric thickness (in km, from [30]) and asthenospheric low-viscosity zone (grey, from [29,30]) derived from seismological observations.

gravitational relaxation [26,25]. Rigid boundary conditions are applied to the bottom and sides, which surround the area of interest with a margin of 63 500 km on each side. The validity of the finite-element model to predict glacial isostatic adjustment has been shown previously [27].

Our earth models consist of an elastic lithosphere, a viscoelastic asthenosphere and an underlying viscoelastic mantle. Density, shear and bulk modulus are volume-averaged values derived from PREM [28]. In the radial direction, upper and lower mantle viscosities are fixed to 3.6×10^{20} and 1.7×10^{22} Pa s, respectively, which is in accordance with forward modelling results from [7] for the Fennoscandian region. The elastic lithosphere has an infinite viscosity, but we have checked the influence of a high, but finite viscosity (down to 10^{24} Pa s) on the model predictions, and found no significant difference for the loading periods considered.

For the generation of synthetic data, we have adopted two 3D reference models (Fig. 1): Model L4 with lateral variations in lithospheric thickness only. The lithospheric thickness increases from 90 km in the North Sea and North Atlantic region to

170 km underneath central Fennoscandia. The average thickness of the entire area is 104 km, while the average thickness underneath the central and peripheral areas is 152 and 92 km, respectively. Model L5 has lateral variations both in lithospheric thickness and asthenospheric viscosity. The lithospheric thickness variation is as in model L4, and a 100 km thick low-viscosity asthenosphere with 10^{18} Pa s is present outside the Baltic Shield (mainly oceanic areas), but absent underneath the cratonic area. The lateral variations are based on seismological evidence [29,30], and are supported by more recent estimates from p- and s-wave tomography [31] and from thermal lithosphere modeling [32]. More details can be found in [20]. Lateral variations deeper in the mantle are not considered in this paper. There are two reasons for this choice: firstly, little reliable evidence for lateral variations in the lowermost upper mantle and the lower mantle is present, except for large-scale variations from global tomography. Secondly, we have shown previously [19] that lateral viscosity variations in the lower mantle have little effect on the prediction of RSL variations in Fennoscandia.

In Fig. 2, two typical radial viscosity profiles for each of the 3D reference models are redrawn. For model L4, only the lithospheric thickness changed from 170 km underneath the continental areas (thick lines) to 90 km underneath the oceanic areas (thin lines). For model L5, an additional pronounced low-viscosity asthenosphere is present underneath the oceanic area (grey area). We then
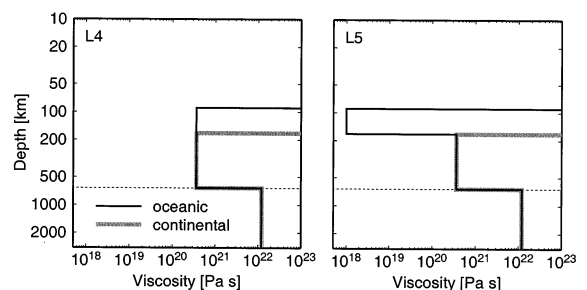

Fig. 2. Typical radial viscosity profiles for the assumed lateral variations for *oceanic areas* (thin lines) and *continental areas* (thick lines) for reference earth models L4 and L5. The dotted lines indicate the 670 km seismic discontinuity.
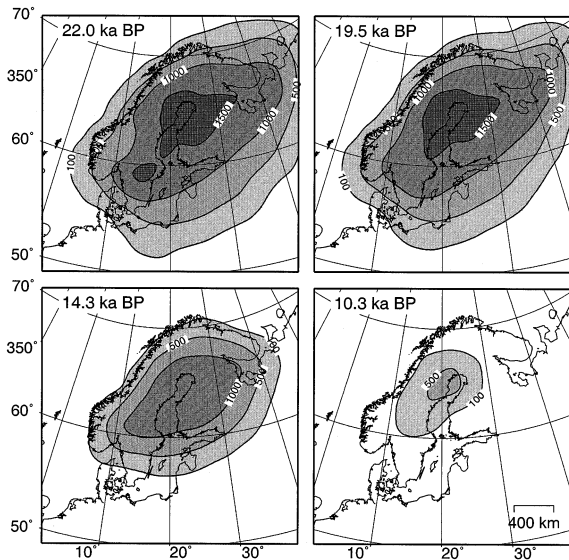
Fig. 3. Ice model FBK8 over Fennoscandia at four different epochs. Contours are drawn every 500 m.

compared the synthetic data generated with the 3D reference models to model predictions based on 1D model, which have two free parameters, the lithospheric thickness and the asthenospheric viscosity. For these 1D models, earth properties vary in the radial direction only.

2.2. Ice model

The ice load model FBK8 (Fig. 3) used in this approach has been derived by [7] from forward modelling predictions of RSL change in Northern Europe. The ice model encompasses two glacial cycles and reached its maximum extent at the last glacial maximum (LGM) at around 22 ka BP. The deglaciation history throughout the Late Pleistocene is based on ice retreat isochrons from [33,34]. Deglaciation ended around 9 ka BP. Lambeck et al. [7] inferred the ice thickness by a least-squares fit of the RSL observations, and the resulting model is characterised by a relatively modest maximum ice height of around 1800 m at the LGM. The ice model of [7] has been modified to match the coarser finite-element grid, which has 225 four-node bilinear elements on the surface with dimensions of 200 km over the area of interest. In the finite-element implementa-

tion, the ice volume is 3.3×10^6 km^3, corresponding to 9.6 m of eustatic sea-level rise.

2.3. RSL data

For the comparison of different model predictions, we define a set of RSL locations in the Fennoscandian region. The site locations are taken from a database used in [35], and contain 40 RSL sites (567 Paleo-coastlines). Fig. 4 shows the irregular distribution of available sea-level data. We define two regions of interest, a *central* area around the Bothnian Bay, encircled by the solid line in Fig. 4, and a *peripheral* area as the rest of the model domain. The central area holds seven RSL locations (176 Paleo-coastlines), the peripheral area holds 33 RSL locations (391 Paleo-coastlines), mainly along the westward (coastal) site of Fennoscandia. At each site, we sample the synthetic sea-level data o_i at the original observation times t_i given in the database. We then assign the original observational uncertainty Δo_i to each synthetic sea-level datum o_i. Typical values of the observational uncertainty range from $\Delta o_i = 2$ m for times younger than 4000 years to $\Delta o_i = 10$–15 m for times older than 10 000 years.
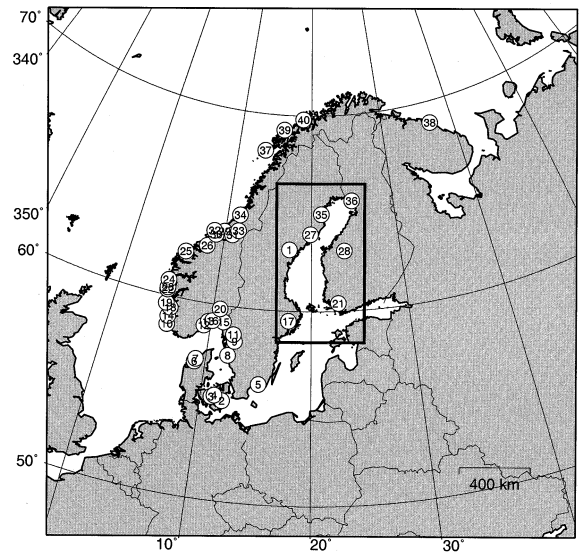

Fig. 4. Location map of Fennoscandia, with 40 RSL sites marked as dots. The area enclosed by the rectangle is defined as *central area*, the area outside as *peripheral area*.

Table 1
Parameters of the best-fitting 1D earth models, with h the lithospheric thickness, η the asthenospheric viscosity, and RMS_{op} the square root of the misfit

		L4	L5	L4a	L5a	L4b	L5b
All	h (km)	110	100	110	40	130	80
	η (Pa s)	3.6×10^{20}	3.6×10^{20}	3.6×10^{20}	3.6×10^{20}	3.6×10^{20}	3.6×10^{20}
	RMS_{op}	0.75	2.17	1.26	2.60	0.71	2.09
Central	h (km)	130	130	150	90	130	60
	η (Pa s)	3.6×10^{20}	3.6×10^{20}	3.6×10^{20}	3.6×10^{20}	3.6×10^{20}	3.6×10^{20}
	RMS_{op}	0.52	1.67	0.96	1.86	1.11	2.29
Peripheral	h (km)	100	60	100	100	130	150
	η (Pa s)	3.6×10^{20}	3.6×10^{20}	3.6×10^{20}	10^{20}	3.6×10^{20}	3.6×10^{20}
	RMS_{op}	0.65	2.10	0.51	1.34	0.70	2.02

Synthetic 3D earth models are L4 and L5 (observational space and time distribution), L4a and L5a (gridded time distribution), and L4b and L5b (gridded space and time distribution).

Hence, we only replace the sea-level data o_i of the original dataset by synthetic values, and both the temporal and spatial data distribution and the data uncertainties remain unchanged. With this approach, we are able to simulate the resolving power of a realistic sea-level data set for lateral variations in mantle properties.

We predict RSL changes p_i at the RSL sites for various 1D models, and we compare the predictions to our synthetic data using the square root of the least-squares criterion:

$$RMS_{op} = \sqrt{\frac{1}{n}\sum_i \left(\frac{o_i - p_i}{\Delta o_i}\right)^2} \qquad (2)$$

with $i = 1$, n the number of predictions, o_i and Δo_i are the synthetic sea-level data based on the 3D reference models and their uncertainties, and p_i are the predictions based on 1D models. The best-fitting prediction p_i^* is characterised by a minimum value for RMS_{op}. However, several model predictions can satisfy the synthetic data within the given observational uncertainties. Hence, we evaluate a second statistical property:

$$RMS_{pp} = \sqrt{\frac{1}{n}\sum_i \left(\frac{p_i^* - p_i}{\Delta o_i}\right)^2} \qquad (3)$$

with p_i^* the best-fitting model prediction inferred from Eq. 2. For $RMS_{pp} \leq 1$, model prediction p_i fits, on average, the synthetic data as well as the best-fitting model prediction p_i^*.

3. Results

In this section, we invert the synthetic RSL data generated for either 3D earth model L4 or L5 for the best-fitting 1D earth model. As we are interested in separating the effects of lateral lithospheric thickness variations and asthenospheric viscosity variations, we discuss inversions for both synthetic earth models L4 and L5 separately. For all inversions, we assume that the ice model is known, hence uncertainties in the ice load history are not taken into account. Best-fitting 1D earth models are summarized in Table 1.

3.1. Synthetic RSL data for model L4

In Fig. 5, the misfit criterion (Eq. 2) for synthetic model L4 is mapped as a function of lithospheric thickness h and asthenospheric viscosity η for a set of 1D model predictions. In Fig. 5a, all RSL data for all times are considered for the misfit. With $RMS_{op} = 0.75$ (see Table 1), the minimum misfit well explains the synthetic data and is clearly defined in terms of a 1D model with average values of $\bar{h} = 110$ km and $\bar{\eta} = 3.6 \times 10^{20}$ Pa s. Within the observational data uncertainty Δo_i, similarly good predictions are achieved for $h \in [70, 160]$ km (the numbers in brackets are the lower and upper bounds for an acceptable fit based on RMS_{pp}) and η narrowly constrained to 3.6×10^{20} Pa s. Hence, an interpretation with 1D earth models infers the average lithospheric thickness of the synthetic model L4 within the error

bounds of the data, and also predicts the viscosity in the asthenospheric layer. When we restrict the RSL data to the last 8000 years (corresponding to the postglacial period in Fennoscandia) as in Fig. 5b, the inference of an average lithospheric thickness becomes less bounded, but still with $\bar{h} = 130$ km and $\bar{\eta} = 3.6 \times 10^{20}$ Pa s the 1D earth model yields a reasonable average.

We now examine the regional variability of the best-fitting solution by subdividing the synthetic data into the previously defined central and peripheral areas. In Fig. 5c, the misfit criterion for RSL predictions of the central area is mapped. A clear and pronounced minimum with $\mathrm{RMS}_{op} = 0.52$ is found for $\bar{h} = 130$ km (ranges within [80,170] km) and $\bar{\eta} = 3.6 \times 10^{20}$ Pa s. Hence, RSL data from the central area tend to favour a thicker lithosphere, as the sites are located above the thick part of the craton. The RSL data from the peripheral area (Fig. 5d) favour a thinner lithosphere with $\bar{h} = 100$ km (ranges within
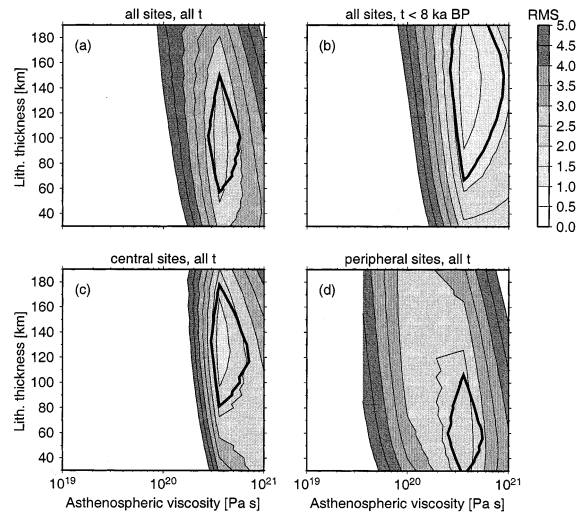

Fig. 5. Map of the square root of the least-squares misfit RMS_{op} as a function of asthenospheric viscosity and lithospheric thickness for reference model L4 and different data subsets: (a) all RSL sites and all times, (b) all RSL sites and times from 8000 years on, (c) central RSL sites and all times, and (d) peripheral RSL sites and all times. The thick black lines encompass models that fit the data as well as the best-fitting model within the observational uncertainties ($\mathrm{RMS}_{pp} \lesssim 1$).

Fig. 6. As Fig. 5, but for reference model L5.

[60,150] km) and $\bar{\eta} = 3.6 \times 10^{20}$ Pa s, with a minimum misfit of $\mathrm{RMS}_{op} = 0.65$.

3.2. Synthetic RSL data for model L5

We now use the synthetic model L5, which includes lateral variations in lithospheric thickness and asthenospheric viscosity. In Fig. 6, misfits between model predictions and synthetic data are mapped. If we invert all RSL data for the 1D model predictions (Fig. 6a), we obtain a best solution for $\bar{h} = 100$ km (ranges are [60,150] km) and $\bar{\eta} = 3.6 \times 10^{20}$ Pa s. However, the best misfit is only $\mathrm{RMS}_{op} = 2.17$ (see Table 1), hence the 1D models cannot explain the synthetic data satisfactorily. We note that the misfit map gives no indication of the low-viscosity asthenosphere, except the poor misfit value. When we invert only for the central RSL data (Fig. 6c), the best misfit is $\mathrm{RMS}_{op} = 1.67$ and the lithospheric thickness is slightly underestimated with $\bar{h} = 130$ km (ranges within [80,170] km), while we find no pronounced asthenosphere underneath the central area. Using only the peripheral RSL data (Fig. 6d), our best inference results in a rather poor misfit of $\mathrm{RMS}_{op} = 2.10$ and a lithospheric thickness of $\bar{h} = 60$ km (ranges within [30,100] km), but the best inversion indicates no lower than average
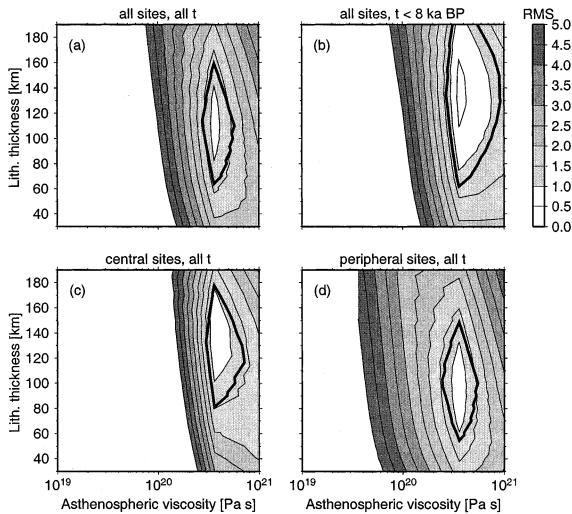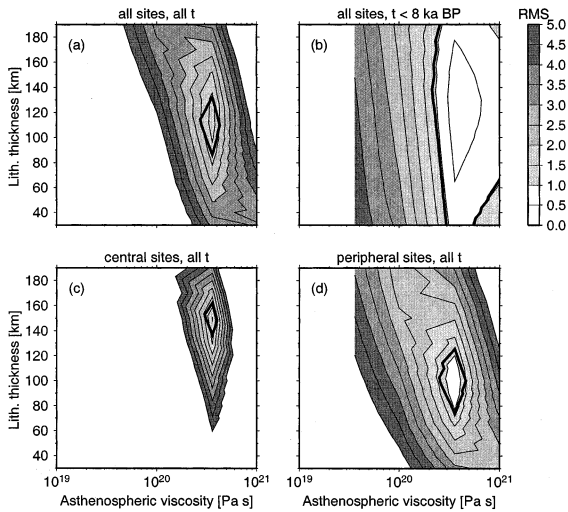
Fig. 7. As Fig. 5, but for reference model L4a and RSL data with time sampled at regular intervals, and a common data uncertainty of $\Delta o_i = 5$ m.

viscosity in the asthenosphere, ($\bar{\eta} = 3.6 \times 10^{20}$ Pa s). Again, the poor reduction in misfit might be a clue for the low-viscosity asthenosphere, together with the wider spacing of the misfit contours. Hence, for the best prediction the model does not indicate a low-viscosity asthenosphere, but it reduces the apparent lithospheric thickness in the peripheral area. We can interpret this behaviour as hiding the low-viscosity asthenosphere in a lithosphere, whose lower part is not elastic, but viscoelastic.

3.3. Synthetic RSL data with gridded times for model L4a

We now sample the RSL data in 1000 year time intervals from the LGM to the present, and we assign a common sea-level observational uncertainty of $\Delta o_i = 5$ m. With this scenario, we simulate a data set of much better quality, reflected in more sampling points and a lower uncertainty expecially for older data. Inverting for the 3D earth model L4a and using all RSL data (Fig. 7a), the best model achieves a misfit of $RMS_{op} = 1.26$, and average values of $\bar{h} = 110$ km and $\bar{\eta} = 3.6 \times 10^{20}$ Pa s, respectively, which is similar to Fig. 5a. However, the lithospheric thickness uncertainty

is significantly reduced to [90,130] km, and the average lithospheric thickness matches the true value for the entire model domain. Restricting the RSL data to the postglacial period (Fig. 7b), we are unable to bound the lithospheric thickness within the interval searched. For the central RSL data (Fig. 7c), we find $\bar{h} = 150$ km and $\bar{\eta} = 3.6 \times 10^{20}$ Pa s, and a misfit value of 0.96. Again, the uncertainties for $\bar{h}$ are reduced to [140,160] km, the best lithospheric thickness estimate is close to the true value for the central area. The peripheral RSL data favour a lithospheric thickness of $\bar{h} = 100$ km, with tight bounds around [80,120] km, and a misfit value of $RMS_{op} = 0.51$.

3.4. Synthetic RSL data with gridded times for model L5a

More interesting is the case of the inversion for synthetic 3D earth model L5a and the RSL data with regular time sampling. Here, the presence of the low-viscosity asthenosphere significantly modifies the inversion. Using the entire RSL data set (Fig. 8a), a poor misfit reduction of $RMS_{op} = 2.60$ is achieved, with a broader minimum misfit. The favoured 1D earth model wrongly predicts a small lithospheric thickness
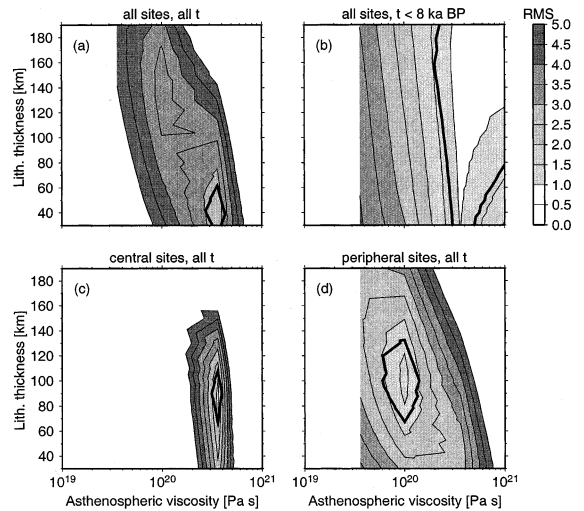

Fig. 8. As Fig. 5, but for reference model L5a and RSL data with time sampled at regular intervals, and a common data uncertainty of $\Delta o_i = 5$ m.
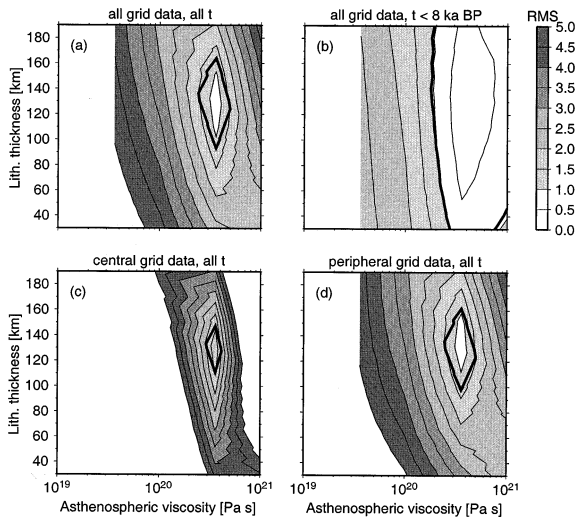
Fig. 9. As Fig. 5, but for reference model L4b and RSL data with locations and time sampled at regular intervals, and a common data uncertainty of $\Delta o_i = 5$ m.

of $\bar{h} = 40$ km, while the broad minimum misfit can be taken as a sign for the low-viscosity asthenosphere. Again, restricting the RSL data to postglacial times results in an unbounded value for the lithospheric thickness (Fig. 8b). The central RSL data (Fig. 8c) wrongly favour a thin lithosphere ($\bar{h} = 90$ km) and no low-viscosity asthenosphere, but again with $RMS_{op} = 1.86$ the minimum misfit is rather poor. However, using the peripheral RSL data (Fig. 8d), the inversion for the first time picks up a signal from the low-viscosity asthenosphere, favouring values of $\bar{h} = 100$ km for the lithospheric thickness and $\bar{\eta} = 10^{20}$ Pa s for the asthenospheric viscosity. With $RMS_{op} = 1.34$ the misfit reduction is better than in Fig. 6d. Hence, for the peripheral data the better sampling of the sea-level data, together with tighter constraints on the observational uncertainty of older data, improves the inversion result.

3.5. Synthetic RSL data with gridded locations and times for model L4b

We now investigate the dependence of the inverse inferences on the spatial sampling of data sites. Instead of using real RSL data sites with their irregular distribution as in the previous sec-

tion, we sample RSL data over the region of interest on a regular grid with a spacing of 100 km, and use the 1000 year time intervals as defined before. Hence, the eastern part of the Baltic Shield (Finland, Russia) is as well sampled as the western coastal part of Fennoscandia, and the central area has more sampling points than in Sections 3.1–3.4.

For this choice of grid data and 3D reference model L4b, misfit maps are shown in Fig. 9. Using all grid data and all times (Fig. 9a), the best misfit with $RMS_{op} = 0.71$ is found for a lithospheric thickness of $\bar{h} = 130$ km (ranges within [90,160] km) and a well constrained asthenospheric viscosity of $\bar{\eta} = 3.6 \times 10^{20}$ Pa s. The range for the lithospheric thickness is similar to the example with real RSL data (L4). Restricting the inversion to postglacial times (Fig. 9b) again results in an unbounded lithospheric thickness. The inversion for grid data from the central area (Fig. 9c) is similar to the result for real RSL data, with $RMS_{op} = 1.11$ and $\bar{h} = 130$ km (ranges within [110,150] km). Differences appear for the grid data from the peripheral area (Fig. 9d). As we sample evenly above the oceanic and cratonic parts, we find an average lithospheric thickness of $\bar{h} = 130$ km (ranges within [100,160] km), which reflects the high sampling density over the thicker, eastern part of the craton. By choosing many grid points further away from the former ice load, we can reduce the misfit to a good fit, $RMS_{op} = 0.70$.

3.6. Synthetic RSL data with gridded locations and times for model L5b

Performing the analysis with gridded data for 3D reference model L5b, and using all grid data and all times (Fig. 10a), the average lithospheric thickness is again not recovered ($\bar{h} = 80$ km, ranging within [50,110] km). The presence of a low-viscosity asthenosphere is visible in the wider contour lines of the grid data inversion. In the central grid data (Fig. 10c), lithospheric thickness is too low with $\bar{h} = 60$ km (ranges within [40,80] km), a hint that the inversion again hides the low-viscosity asthenosphere in a thinner elastic lithosphere. The peripheral grid data with their even sampling again recover a thick lithosphere with $\bar{h} = 160$ km
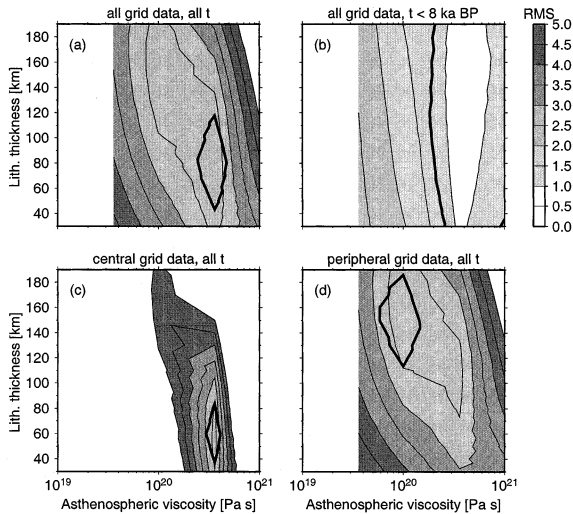
Fig. 10. As Fig. 5, but for reference model L5b and RSL data with locations and time sampled at regular intervals, and a common data uncertainty of $\Delta o_i = 5$ m.

(ranges within [120,180] km), but the minimum misfit also reveals a low-viscosity asthenosphere with values around $\eta = 10^{20}$ Pa s.

4. Discussion

We have inverted synthetic RSL data generated with a 3D earth model for the Fennoscandian region for the best 1D radial viscosity profile.

Our results suggest that the choice of sea-level sites is a controlling parameter for the inversion. As real sea-level data are focused around the coastal margins, the inversion of these data will reveal information on mantle rheology mainly sensitive to these sampling regions. Lateral variations in mantle properties can only be found, when we group the sea-level data into subregions, which might be based on information from seismology or geology.

If the lateral variations would be restricted to changes in lithospheric thickness, they could in principle be detected with 1D earth models. However, as lateral changes in lithospheric thickness are likely to be accompanied by lateral viscosity variations, e.g. low-viscosity asthenospheric regions underneath oceanic regions, 1D earth models fail to correctly predict absolute values for lithospheric thickness and asthenospheric viscosities. This result is in agreement with our previous modelling of the forward problem [13,15,18,20].

The failure to pick up the signal from a low-viscosity asthenosphere is mainly attributable to the fact that in Fennoscandia sea-level data in the vicinity of the low-viscosity zone are peripheral sea-level sites, whose amplitude is small (e.g. tens of metres), when compared to the central sea-level data (e.g. hundreds of metres). Hence, the observational uncertainties of peripheral sea-level data, which are in the order of the data itself for late-glacial times, prevent a proper resolution of mantle viscosity along the coastal areas. We have shown that only significantly improved observations of sea-level change in the peripheral area would be able to resolve the low-viscosity asthenosphere, but even then the inversion will only be qualitative.

References

[1] W.R. Peltier, The impulse response of a Maxwell Earth, Rev. Geophys. Space Sci. 12 (1974) 649–669.

[2] W.E. Farrell, J.A. Clark, On postglacial sea level, Geophys. J. R. Astron. Soc. 46 (1976) 647–667.

[3] J.X. Mitrovica, J.L. Davis, I.I. Shapiro, A spectral formalism for computing three-dimensional deformations due to surface loads 1. Theory, J. Geophys. Res. 99 (1994) 7057–7073.

[4] G.A. Milne, J.X. Mitrovica, Postglacial sea-level change on a rotating Earth, Geophys. J. Int. 133 (1998) 1–19.

[5] J.X. Mitrovica, J.L. Davis, I.I. Shapiro, A spectral formalism for computing three-dimensional deformations due to surface loads 2. Present-day glacial isostatic adjustment, J. Geophys. Res. 99 (1994) 7075–7101.

[6] W.R. Peltier, Mantle viscosity and ice-age ice sheet topography, Science 273 (1996) 1359–1364.

[7] K. Lambeck, C. Smither, P. Johnston, Sea-level change,

glacial rebound and mantle viscosity for northern Europe, Geophys. J. Int. 134 (1998) 102–144.

[8] W. Su, A.M. Dziewonski, Predominance of long-wavelength heterogeneity in the mantle, Nature 352 (1991) 121–126.

[9] X.D. Li, B. Romanowicz, Global mantle shear velocity model developed using nonlinear asymptotic coupling theory, J. Geophys. Res. 101 (1996) 22245–22272.

[10] J. Trompert, Global seismic tomography the inverse problem and beyond, Inverse Probl. 14 (1998) 371–385.

[11] R. Sabadini, P. Gasperini, Glacial isostasy and the interplay between upper and lower mantle lateral viscosity heterogeneities, Geophys. Res. Lett. 16 (1989) 429–432.

[12] P. Gasperini, R. Sabadini, Lateral heterogeneities in mantle viscosity and post-glacial rebound, Geophys. J. 98 (1989) 413–428.

[13] G. Kaufmann, P. Wu, D. Wolf, Some effects of lateral heterogeneities in the upper mantle on postglacial land uplift close to continental margins, Geophys. J. Int. 128 (1997) 175–187.

[14] C. Giunchi, G. Spada, R. Sabadini, Lateral viscosity variations and postglacial rebound: effects on present-day VLBI baseline deformations, Geophys. Res. Lett. 24 (1997) 13–16.

[15] G. Kaufmann, P. Wu, Upper mantle lateral viscosity variations and postglacial rebound: application to the Barents Sea, in: P. Wu (Ed.), Dynamics of the Ice Age Earth: a Modern Perspective, Trans Tech Pub., Zürich, 1998, pp. 583–602.

[16] Z. Ni, P. Wu, Effects of removing concentric positioning on postglacial vertical displacement in the presence of lateral variation in lithospheric thickness, Geophys. Res. Lett. 25 (1998) 3209–3212.

[17] Z. Martinec, O. Čadek, L. Fleitout, Can the 1D viscosity profiles inferred from postglacial rebound data be affected by lateral changes in the lithospheric thickness?, Geophys. Res. Lett. 28 (2001) 4403–4406.

[18] G. Kaufmann, P. Wu, Lateral asthenospheric viscosity variations and postglacial rebound: a case study for the Barents Sea, Geophys. Res. Lett. 25 (1998) 1963–1966.

[19] P. Wu, Z. Ni, G. Kaufmann, Postglacial rebound with lateral heterogeneities: from 2D to 3D modeling. in: P. Wu (Ed.), Dynamics of the Ice Age Earth: a Modern Perspective, Trans Tech Pub., Zürich, 1998, pp. 557–582.

[20] G. Kaufmann, P. Wu, G. Li, Glacial isostatic adjustment in Fennoscandia for a laterally heterogeneous Earth, Geophys. J. Int. 143 (2000) 262–273.

[21] G. Kaufmann, P. Wu, Glacial isostatic adjustment on a three-dimensional earth: examples from Fennoscandia

and the Barents Sea, in: J.X. Mitrovica, L.L.A. Vermeersen (Eds.), Sea-level, Crustal Deformation, Gravity and Rotation, AGU Geodynamics Series, 2002, pp. 1–7.

[22] D. Wolf, The relaxation of spherical and flat Maxwell Earth models and effects due to the presence of the lithosphere, J. Geophys. 56 (1984) 24–33.

[23] F. Amelung, D. Wolf, Viscoelastic perturbations of the Earth: significance of the incremental gravitational force in models of glacial isostasy, Geophys. J. Int. 117 (1994) 864–879.

[24] P. Wu, Deformation of an incompressible viscoelastic flat Earth with power-law creep: a finite element approach, Geophys. J. Int. 108 (1992) 35–51.

[25] P. Wu, Viscoelastic versus viscous deformation and the advection of pre-stress, Geophys. J. Int. 108 (1992) 136–142.

[26] P. Wu, W.R. Peltier, Viscous gravitational relaxation, Geophys. J. R. Astron. Soc. 70 (1982) 435–485.

[27] P. Wu, P. Johnston, Validity of using flat-earth finite element models in the study of postglacial rebound, in: P. Wu (Ed.), Dynamics of the Ice Age Earth: a Modern Perspective, Trans Tech Pub., Zürich, 1998, pp. 191–202.

[28] A.M. Dziewonski, D.L. Anderson, Preliminary reference Earth model, Phys. Earth Planet. Inter. 25 (1981) 279–356.

[29] G.F. Panza, S. Mueller, G. Calcagnile, The gross features of the lithosphere-asthenosphere system in Europe from seismic surface waves and body waves, Pure Appl. Geophys. 118 (1980) 1209–1213.

[30] G. Calcagnile, The lithosphere–asthenosphere system in Fennoscandia, Tectonophys. 90 (1982) 19–35.

[31] S. Goes, R. Govers, Shallow mantle temperatures under Europe from *P* and *S* wave tomography, J. Geophys. Res. 105 (2000) 11153–11169.

[32] I.M. Artemieva, W.D. Mooney, Thermal thickness and evolution of Precambrian lithosphere: a global study, J. Geophys. Res. 106 (2001) 16387–16414.

[33] B.G. Andersen, Barents Sea and Arctic islands, in: G.H. Denton, T.J. Hughes (Eds.), The Last Great Ice Sheets, Wiley, New York, 1981, pp. 41–45.

[34] S.S. Pedersen, Israndslinier i norden, Technical report, Danm. Geol. Unders., 1995.

[35] G. Kaufmann, K. Lambeck, Mantle dynamics, postglacial rebound and the radial viscosity profile, Phys. Earth Planet. Sci. 121 (2000) 303–327.

[36] P. Wessel, W.H.F. Smith, Free software helps map and display data, EOS 72 (1991) 441–446.

[37] P. Wessel, W.H.F. Smith, New, improved version of Generic Mapping Tools released, EOS 79 (1998) 579.